ADVANCED ENGINEERING MATERIALS
www.aem-journal.com

Single-Crystal Castability of CM186LC Nickel-Based Superalloy

*André Baldissera, Sean Böhm, Rainer Völkl, and Uwe Glatzel**

Appropriate conditions to obtain single-crystal (SX) castings of the nickel-based superalloy CM186LC, developed for directional solidification, are investigated. Cylindrical samples with starter blocks and grain selectors are cast via a proprietary SX Bridgman process. The effect of the solidification rates (V) ranging from 1 to 10 mm·min^{-1} on the microstructure is explored. Primary dendrite arm spacings (λ_p) fall within the expected range of 200–500 µm. Single crystal is achieved at $V \cong 3$ mm·min^{-1}. The growth direction of the crystals in all cases diverges strongly from [001] orientation. Different solidification behavior of CM186LC compared to otherwise chemically similar CMSX-4 is attributed to minor additions of grain boundary strengtheners C, Hf, B, and Zr.

1. Introduction

The historical development of nickel-based superalloys is affected by increasing the volume fraction of the strengthening γ′ phase accompanied by evolving casting technologies.[1] Pouring a superalloy melt into a shell mold on a cooled chill plate enabled directional heat conduction and, therefore, directional solidification (DS) resulting in elongated and directional grain structures.[2] Grain boundary strengtheners like C, B, Zr, and Hf are often added to DS superalloys. The development culminated in tailored compositions to cast single crystalline (SX) superalloy parts. Thus, grain boundary strengtheners are usually not found in these dedicated SX superalloys.[3] Burkholder et al.[4] stated that high-purity, ultrahigh creep, and fatigue strength SX alloys are limited to low-angle boundaries (LABs), which typically not exceed 6° in critical airfoil locations. Technically speaking, parts made from these SX superalloys are considered scrap if LABs exceed 6°.

From the side of evolving casting technologies,[1] SX superalloy parts became possible through the development of dedicated Bridgman process.[5] A ceramic shell mold is built-on a lost model of the superalloy part with an added so-called grain selector and a starter.[6] The shell mold with the superalloy melt in it is withdrawn vertically from a hot zone down to a cold zone to start directional solidification. In such a Bridgman furnace the solidification rate of the mold is controlled. An interchanging use of the terms withdrawal rate and solidification rate in literature is confusing. However, under most circumstances, withdrawal rate and solidification rate are closely related.

Table 1 shows the chemical composition of the CM186LC, a second-generation nickel-based superalloy with 3% Re. The superalloy CM186LC was developed with directional solidification in mind.[7] It therefore contains the known grain boundary strengtheners Hf, B, and Zr. The combined Al, Ti, and Ta content of ≈9.5% enables high γ′ phase volume fraction. Creep strength is elevated by alloying with the refractory elements 3% Re and 8% W. CM186LC could be readily cast into aero turbine multi-airfoil segments. Mechanical property and turbine engine testing proved that the CM186LC could accommodate LABs up to 30° resulting in high casting yields.[4]

Even though CM186LC is not a dedicated SX superalloy, researchers saw in this alloy a cost-effective opportunity to produce SX equivalent parts of high geometric complexity. CM186LC master alloy can be readily produced from casting scraps of the superalloys CMSX-2, −3, or −4,[8] thus contributing to the economic aspect. Among these superalloys all developed by the Cannon-Muskegon Corporation, CMSX-4 exhibits the greatest similarities to CM186LC. Table 1 gives the chemical compositions of CM186LC and CMSX-4. Both superalloys have astonishing close major alloying element contents. In a technological sense CM186LC is CMSX-4 with small additions of C, Hf, B, and Zr.

Although it is possible to cast CM186LC SX complex parts, the processing conditions to achieve single crystals are less understood. In the Bridgman process precise control over solidification parameters is essential. Adjusting solidification rates (V) helps achieving uniform dendrite formation, thereby reducing the likelihood of LABs. Therefore, this work investigates these conditions and explores the effect of the solidification rates on the microstructure and SX castability of CM186LC.

2. Experimental Section

Figure 1 illustrates the sample manufacturing process. Cylindrical positive models (15 mm in diameter and 90 mm in length) were

A. Baldissera, S. Böhm, R. Völkl, U. Glatzel
Metals and Alloys
University of Bayreuth
Prof.-Rüdiger-Bormann-Str. 1, 95447 Bayreuth, Germany
E-mail: uwe.glatzel@uni-bayreuth.de

The ORCID identification number(s) for the author(s) of this article can be found under https://doi.org/10.1002/adem.202500837.

DOI: 10.1002/adem.202500837

Table 1. Chemical composition of CM186LC[4] and CMSX-4.[14]

Elements in wt.%	Ni	C	Cr	Al	Co	Mo	Ti	Ta	Re	B	W	Hf	Zr
CM186LC	Bal	0.07	6.0	5.7	9.0	0.5	0.7	3.0	3.0	0.015	8.0	1.4	0.005
CMSX-4	Bal	–	6.5	5.6	9.0	0.6	1.0	6.5	3.0	–	6.0	<0.1	–

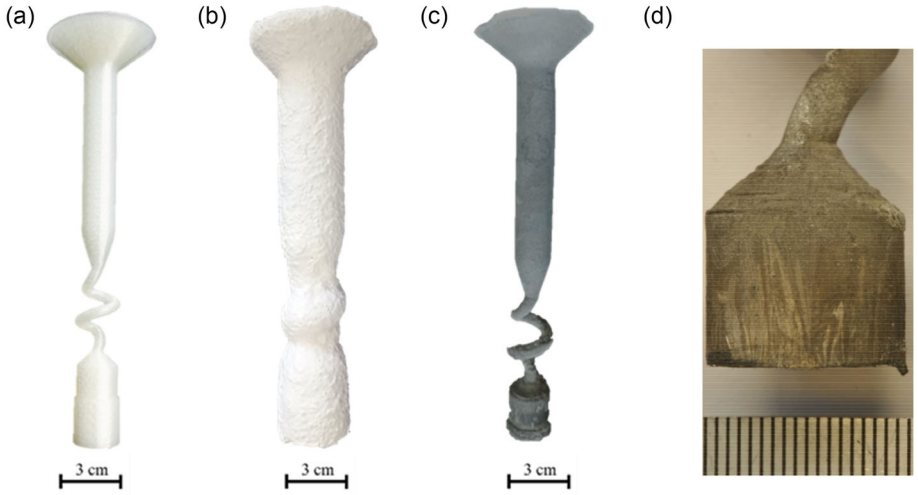

Figure 1. Sample manufacturing steps: a) 3D-printed positive model; b) ceramic shell; c) as-cast sample; and d) macro image of the starter of a CM186LC casting solidified at a rate of 1 mm min^{-1}. Fine equiaxed grains at the bottom; thereafter columnar grains, tilted in respect to the vertical.

3D-printed using the fused deposition modeling (FDM) technique with polyvinyl butyral filament (PVB).[9] The helical grain selector was a diameter of 5 mm and a single winding of 360° over a length of 40 mm. Alternately dipped the PVB model into a ceramic slurry, followed by sanding the model with ceramic powder or stucco, resulting in the application of nine layers. The shell was dried after every new layer. The inner three layers were composed of alumina (Al_2O_3) sand of 0.1 mm grain size, followed by three layers of alumina sand of 0.25 mm grain size, and finally three layers of alumina sand of 0.5 mm grain size. The sole ceramic slurry contained binding agents and a mixture of zircon ($ZrSiO_4$) and silica (SiO_2). The shell was heated to 450 °C to remove the polymer and then sintered at 1200 °C, resulting in a ceramic shell with a wall thickness of ≈5 mm.

The CM186LC alloy was melted in a proprietary Bridgman vacuum induction melting furnace.[10] A ceramic zirconium oxide crucible was used to melt ≈200 g of the material. The ceramic shell was positioned over a water-cooled copper chill plate with a diameter of 18 mm, heated to 1450 °C, and molten alloy was poured into it. Using the Bridgman process, V from 1 to 10 mm·min^{-1} were employed for solidification.

Macroetching with Adler's etchant was applied to reveal the presence of grains on the surface of the cast specimens. Subsequently, the samples were cut transversely, and the cross-sections were embedded in phenolic resin, ground with SiC paper (grit sizes ranging from 500 to 1000 µm), polished with diamond suspensions (granulometries of 9, 6, and 3 µm), and finished with a SiO_2 colloidal suspension (0.1 µm). The dendritic structure became visible after etching in a solution of 3 g Mo-(VI) oxide, 100 mL H_2O, 100 mL HNO_3, and 100 mL HCl. Optical microscope micrographs were taken using a Stemi SV 6 stereo microscope and a Zeiss Axioplan 2 light microscope equipped with an Olympus UC30 camera. Grain or single-crystal orientations, respectively, were determined using a scanning electron microscope (Zeiss Sigma 300 VP) and an electron backscatter diffraction detector (EBSD) from EDAX, (Clarity Super).

The growth direction (GD) of crystals in respect to the vertical axis of the proprietary Bridgman furnace is called crystal orientation and is characterized by the nearest zone axis with single-digit indices in the inverse pole figure (IPF). The angle between these two directions is referred to as crystal orientation angle (α). The angle between GD of two individual grains called angled grain boundaries angle (ABs angle) or denominated with angle (β), respectively.

3. Results

Figure 2 presents cross-sectional micrographs of four CM186LC alloy castings. CM186LC solidifies dendritically in the applied V range of 1–10 mm·min^{-1}. It is well established that the formation of regular cruciform dendritic patterns results from dendrite cores growing in alignment with the [001] crystallographic orientation.[11] Primary dendrite arm spacing, λ_p, decreases from 500 to 270 µm while the solidification rate increases by one order of magnitude from 1 to 10 mm·min^{-1} (**Table 2**). Sample d, produced at 10 mm·min^{-1}, exhibits the finest dendritic microstructure. All

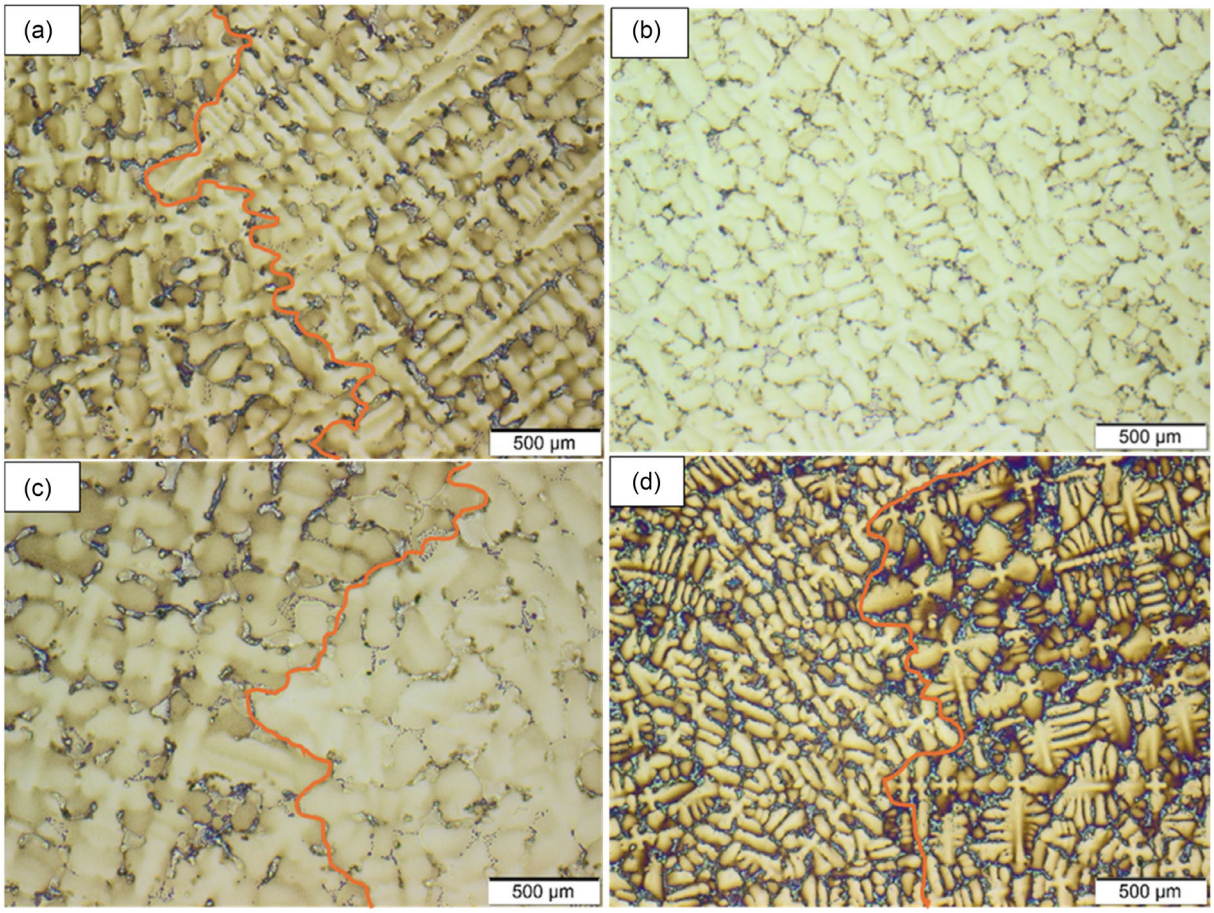

Figure 2. Cross-sectional micrographs of CM186LC alloy castings produced at different solidification rates: grain boundaries are marked by orange lines. a) 1 mm·min^{-1}, oligocrystalline; b) 3 mm·min^{-1},SX; c) 5 mm·min^{-1}, oligocrystalline; and d) 10 mm·min^{-1}, oligocrystalline.

Table 2. CM186LC alloy casting factors and measured structure features.

Sample denomination	V [mm·min^{-1}]	Crystallinity	Crystal orientation α	ABs β	λ_p [µm]
a	1	oligo	10°–50°	10°–40°	500
b	3	single	≈42°	–	420
c	5	oligo	10°–50°	10°–40°	360
d	10	oligo	10°–50°	10°–40°	270

CM186LC alloy castings show large residual γ/γ′ eutectic islands in interdendritic regions.

Samples solidified at 1, 5, and 10 mm·min^{-1} are oligocrystalline. In cross-sectional micrographs of Figure 2, grain boundaries are marked by orange-colored lines. Grain boundaries are elongated in the direction of solidification, that is, normal to the cross-sectional planes shown in Figure 2. The GD of the grains in the oligocrystalline samples deviate strongly from [001] orientation, the direction of fastest crystal growth usually expected from face centered cubic crystals.[12] Crystal orientation angles α vary from ≈10° up to ≈50°. Angles between adjacent grains are observed (β) to range from 10° to 40°.

In contrast, sample b processed at 3 mm·min^{-1} is SX. **Figure 3** shows false-color EBSD maps relative to the GD of CM186LC alloy castings with the corresponding IPF. Single crystals have a degree of texture (Figure 3b), that is, the resultant IPF show the accumulation of poles around one specific orientation.[13] The SX sample b which was solidified at 3 mm·min^{-1} (Figure 3b) is orientated close to [7 4 9], hence a strong deviation of $\alpha \cong 42°$ from [001].

Figure 1d shows the macro image of the starter of the CM186LC casting solidified at a rate of 1 mm·min^{-1}. Fine equiaxed grains are observed at the bottom; thereafter columnar grains are formed, which are tilted in respect to the vertical axis. Figure 1d exemplifies that even at the beginning of solidification, hence at the SX starter block, GD of the grains deviate from [001]. Table 2 summarizes the results taken from the CM186LC alloy castings in this study.

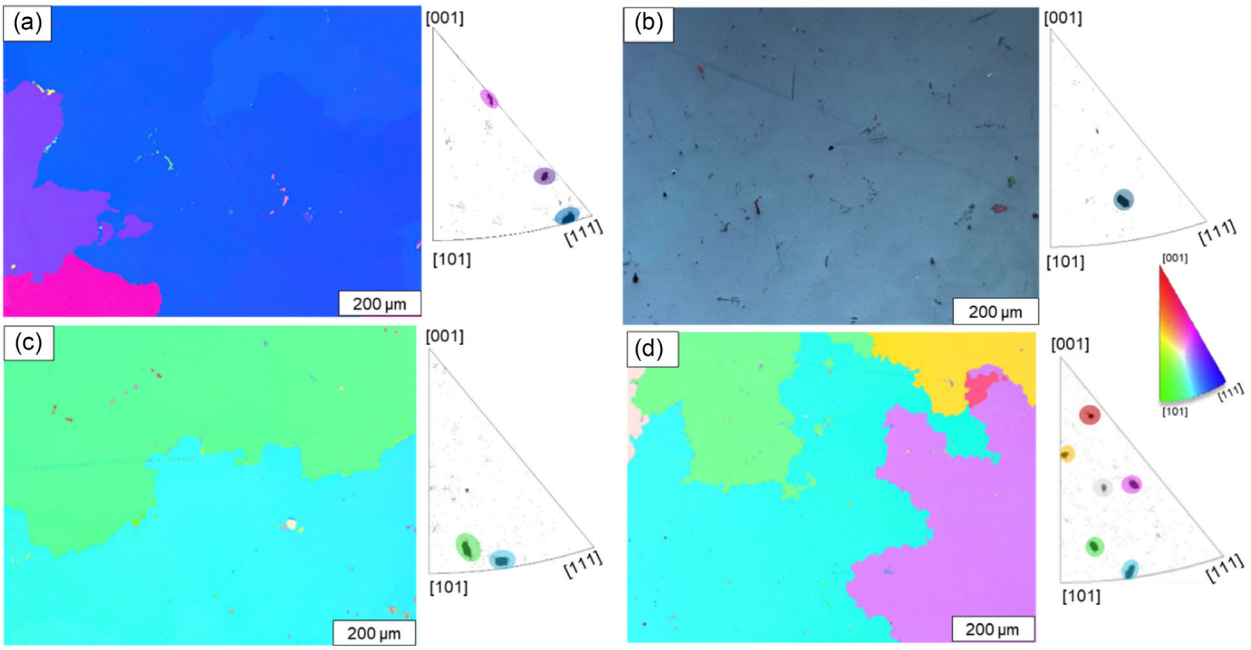

Figure 3. False-color EBSD maps and IPF relative to the GD of the CM186LC alloy castings, produced at different solidification rates: a) 1 mm min^{-1}, oligocrystalline with three grains; b) 3 mm min^{-1},SX; c) 5 mm min^{-1}, oligocrystalline with two grains; and d) 10 mm min^{-1}, oligocrystalline with six grains.

4. Discussion

The temperature gradient at the solidification front (G) and the V are principal factors of single-phase solidification of alloys. In the Bridgman process these two factors can be controlled independently from each other within some ranges. With the proprietary Bridgman furnace for casting cylindrical shaped superalloy ingots with a high aspect ratio, it is straightforward to $\approx V$ by the withdrawal rate of the mold.[14,15]

Solidification morphologies of CM186LC are columnar dendritic in all cases. In the proprietary Bridgman furnace the temperature gradient at the solidification front is determined to be $G \cong 5 \times 10^{-4}$ K m^{-1}. In the here investigated V range of 1–10 mm·min^{-1}, columnar dendritic morphology is often observed in directionally solidified nickel-based superalloys,[16,17] and CM186LC is no exception to this rule of thumb. Also, λ_p from 270 to 500 µm (Table 2) are in the usual range of directionally solidified nickel-based superalloys at solidification rates of $V = 1$–10 mm·min^{-1} and with a temperature gradient of $G \cong 5 \times 10^{-4}$ K m^{-1},[11] that is, in a solidification variables range where columnar dendritic solidification prevails.

Solidification rates of 1–10 mm·min^{-1} are typical for industrial castings of SX parts from for example the dedicated SX superalloy CSMX-4.[14,18,19] Körber et al.[20] casted SX structures with a high yield from a DS alloy MAR M247LC with the here descripted proprietary Bridgman furnace at V from 0.5–6 mm·min^{-1}. CM186LC behaves differently, only in a narrow process window around $V \cong 3$ mm·min^{-1} a single crystal is obtained with otherwise similar process variables than Körber et al.[20] Onyszko et al.[21] casted SX turbine blades by the Bridgman method from CMSX-4 superalloy at various solidification rates between 1 and 5 mm·min^{-1}. Onyszko et al.[21] also found that at 3 mm·min^{-1} the angle of deviation from the [001] direction, that is, the crystal orientation, scattered the least along the Z axis of the blade. At 5 mm·min^{-1}, Onyszko et al.[21] observed however, LABs, that is, subgrains were formed in the otherwise SX blades from CMSX-4. Hence, somehow independent of the casting form and equipment, medium solidification rates around $V \cong 3$ mm·min^{-1} turn out to be optimum for high yield of single-crystal parts from CMSX-4. This tendency was observed in our experiments with the CM186LC alloy, having a closely related chemical composition (see Table 1).

Burkholder et al.[4] concluded that: "The SX castability of the alloy has also exceed expectations, which along with the generous grain specifications with resultant high casting yield and absence of a vacuum solution heat treatment and Rx, result in appreciably lowers manufacturing costs". Mechanical property evaluations and turbine engine testing have shown that CM186LC can tolerate LABs up to 30°, which contributes to high casting yields.[4] In the context of technical single-crystal nickel-based superalloys, crystal lattice misorientation between adjacent regions, that is, LABs, cannot exceed 6° of misorientation.[4] Accordingly, the grain angle boundaries of our SX castings performed at $V \cong 3$ mm·min^{-1} remained under 6°, as bona fide SX structures.

The DS process of superalloys is highly complex, as heat flow, growth velocity, and elemental segregation influence the GD.[22] The additional grain boundary strengtheners in CM186LC seemingly further narrow its process window for SX casting. All signs of this study speak for a more isotropic grain growth rate of CM186LC compared to CMSX-4. Thus, [001] is not the predominant grain GD in CM186LC, which in turn gives rise to a strong deviation of the crystal orientations from [001] and high-angle grain boundaries.

5. Conclusions

The appropriate conditions to obtain actual single crystals from CM186LC, a dedicated DS alloy, comprehend the use of SX starter block and grain selector in conjunction with a narrow process window of $V \cong 3\ \mathrm{mm \cdot min^{-1}}$. The GD of single crystals deviate strongly from the [001] orientation. The SX deviation angle α reached up to ≈40°. Outside of this narrow process window, oligocrystals are formed. The crystallographic orientations of the oligocrystals exhibit deviations ranging from 10° to 50° of the [001]. Oligocrystals show high-angle grain boundaries, with grain boundary angles β ranging from 10° to 40°.

Acknowledgements

The financial support by the German Research Foundation DFG, project number 515779084, reference GL181/70-1, is gratefully acknowledged.

Open Access funding enabled and organized by Projekt DEAL.

Conflict of Interest

The authors declare no conflict of interest.

Author Contributions

André Baldissera: conceptualization (lead); formal analysis (lead); investigation (lead); methodology (lead); visualization (lead); writing—original draft (lead); writing—review & editing (lead). **Sean Böhm**: methodology (supporting); visualization (supporting); writing—original draft (supporting); writing—review & editing (supporting). **Rainer Völkl**: conceptualization (supporting); methodology (supporting); visualization (supporting); writing—original draft (supporting); writing—review & editing (supporting). **Uwe Glatzel**: funding acquisition (lead); resources (lead); writing—original draft (supporting); writing—review & editing (supporting).

Data Availability Statement

The data that support the findings of this study are openly available in Advanced Engineering Materials at http://doi.org/[10.1002/adem.202500837], reference number [ADEM202500837].

Keywords

Bridgman processes, CM186LC, nickel-based superalloys, single crystals, solidification rates

Received: March 26, 2025
Revised: June 4, 2025
Published online: July 21, 2025

[1] R. C. Reed, *The Superalloys – Fundamentals and Applications*, Cambridge University Press, Cambridge **2006**.
[2] F. I. Versnyder, M. E. Shank, *Mater. Sci. Eng.* **1970**, *6*, 213.
[3] *Superalloys 1980 (Fourth Int. Symp.)* (Eds: M. Gell, D. N. Duhl, A. F. Giamei), TMS, Warrendale, Pennsylvania, USA **1980**.
[4] P. S. Burkholder, M. C. Thomas, R. Helmink, D. J. Frasier, K. Harris, J. B. Wahl, *Volume 4: Manufacturing Materials and Metallurgy; Ceramics; Structures and Dynamics; Controls, Diagnostics and Instrumentation; Education; IGTI Scholar Award; General*, American Society of Mechanical Engineers, Indianapolis, Indiana **1999**.
[5] P. W. Bridgman, *Proc. Am. Acad. Arts Sci.* **1925**, *60*, 305.
[6] H. J. Dai, J. C. Gebelin, M. Newell, R. C. Reed, N. D'Souza, P. D. Brown, H. B. Dong, in *Superalloys 2008 (Eleventh Int. Symp.)*, TMS, Warrendale, Pennsylvania, USA **2008**, pp. 367–374.
[7] F. Caruel, S. Bourguignon, B. Lallement, S. Fargeas, A. DeBussac, K. Harris, G. L. Erickson, J. B. Wahl, *J. Eng. Gas Turbines Power* **1998**, *120*, 97.
[8] K. Harris, G. L. Erickson, S. L. Sikkenga, W. D. Brentnall, J. M. Aurrecoechea, K. G. Kubarych, in *Superalloys 1992 (Seventh Int. Symp.)*, TMS, Warrendale, Pennsylvania, USA **1992**, pp. 297–306.
[9] S. Körber, R. Völkl, U. Glatzel, *J. Mater. Process. Technol.* **2021**, *293*, 117095.
[10] C. H. Konrad, M. Brunner, K. Kyrgyzbaev, R. Völkl, U. Glatzel, *J. Mater. Process. Technol.* **2011**, *211*, 181.
[11] B. Chalmers, *Principles of Solidification, Wiley Series on the Science and Technology of Materials*, Wiley, New York, NY **1964**.
[12] W. A. Tiller, *JOM* **1957**, *9*, 847.
[13] H. J. Bunge, H. Bunge, *Texture Analysis in Materials Science – Mathematical Methods*, Butterworths, London **1982**.
[14] K. Gancarczyk, M. Zubko, A. Hanc-Kuczkowska, B. Kościelniak, R. Albrecht, D. Szeliga, M. Motyka, W. Ziaja, J. Sieniawski, *Materials* **2019**, *12*, 3422.
[15] H. S. Whitesell, L. Li, R. A. Overfelt, *Metall. Mater. Trans. B* **2000**, *31*, 546.
[16] P. N. Quested, M. McLean, *Mater. Sci. Eng.* **1984**, *65*, 171.
[17] W. Kurz, D. J. Fisher, *Fundamentals of Solidification*, Trans Tech Publications, Uetikon-Zürich **1998**.
[18] P. Caron, T. Khan, *Aerosp. Sci. Technol.* **1999**, *3*, 513.
[19] A. Kermanpur, M. Rappaz, N. Varahram, P. Davami, *Metall. Mater. Trans. B* **2000**, *31*, 1293.
[20] S. Körber, M. Fleck, R. Völkl, U. Glatzel, *Adv. Eng. Mater.* **2022**, *24*, 2101332.
[21] A. Onyszko, W. Bogdanowicz, K. Kubiak, J. Sieniawski, *Cryst. Res. Technol.* **2010**, *45*, 1326.
[22] A. Wagner, B. A. Shollock, M. McLean, *Mater. Sci. Eng., A* **2004**, *374*, 270.